

# Experimental twin-field quantum key distribution with flawed and correlated sources

Jie Gu,<sup>1,\*</sup> Xiao-Yu Cao,<sup>1,\*</sup> Yao Fu,<sup>2,3</sup> Zong-Wu He,<sup>1,4</sup> Ze-Jie Yin,<sup>4</sup> Hua-Lei Yin,<sup>1,†</sup> and Zeng-Bing Chen<sup>1,3,‡</sup>

<sup>1</sup>*National Laboratory of Solid State Microstructures and School of Physics,  
Collaborative Innovation Center of Advanced Microstructures, Nanjing University, Nanjing 210093, China*

<sup>2</sup>*Beijing National Laboratory for Condensed Matter Physics and Institute of Physics,  
Chinese Academy of Sciences, Beijing 100190, China*

<sup>3</sup>*MatricTime Digital Technology Co. Ltd., Nanjing 211899, China*

<sup>4</sup>*State Key Laboratory of Particle Detection and Electronics,  
University of Science and Technology of China, Hefei 230026, China*

(Dated: April 19, 2022)

The security of quantum key distribution (QKD) is severely threatened by discrepancies between realistic devices and theoretical assumptions. Recently, a significant framework called the reference technique was proposed to provide security against arbitrary source flaws, including pulse correlations. Here, we propose an efficient four-phase twin-field QKD using laser pulses adopting the reference technique for security against all possible source imperfections. We present a characterization of source flaws and connect them to experimental data, together with a finite-key analysis. In addition, we demonstrate the feasibility of our protocol through a proof-of-principle experimental implementation and demonstrate a secure key rate of 1.63 kbps with a 20 dB channel loss. Compared with previous QKD protocols with imperfect devices, our work considerably improves both the secure key rate and the transmission distance, and shows application potential in the practical deployment of secure QKD with device imperfections.

## I. INTRODUCTION

Quantum key distribution (QKD) enables two distant participants, Alice and Bob, to share secure key bits [1, 2] for the encryption and decryption of secret communication. Together with the one-time pad algorithm, QKD offers theoretical security for information exchanges based on the laws of quantum mechanics [3, 4]. However, for the practical operation of QKD systems, a serious security loophole still exists, which occurs due to the discrepancy between theoretical security assumptions and practical devices. To be precise, a security proof of QKD is established with assumptions on the system devices, which cannot be satisfied for realistic devices because of inherent imperfections and the disturbance of eavesdroppers [5–8]. This deviation results in more information leakage to eavesdroppers, which cannot be noticed by users [3].

To narrow the discrepancy and further strengthen the security against device flaws, some crucial protocols have been presented, one of which is device-independent (DI) QKD, which guarantees the unconditional security of QKD by measuring the violation of Bell’s inequality [9]. Although a number of experimental demonstrations of the loophole-free Bell test have been conducted [10–12], experimental implementations of DI-QKD still suffer from short transmission distances, because they require nearly perfect single-photon detection. To date, several DI-QKD experiments have been performed, which show that DI-QKD is still far from being implemented in long-

distance transmission [13–15], as listed in Table. I]. Furthermore, a recent study revealed that Bell nonlocality is insufficient to prove the security of standard DI-QKD protocols [16] in the large-noise regime.

Another significant approach towards the security of practical QKD is measurement-device-independent QKD [17], as well as its single-photon interference version twin-field (TF) QKD [18], which closes all attacks on measurement devices, is practical [19–26], and breaks the transmission record using current technologies [27–31]. Thus, source flaws present a loophole towards securing QKD with imperfect devices. In recent years, several studies have been conducted to improve the security with source flaws, such as the loss-tolerant protocol [32–35] and other attempts [36–41]. Recently, an important theoretical work was published to propose a security analysis method for practical QKD against source flaws, which is called the reference technique (RT) [42]. Using the RT method, parameters characterizing typical source flaws, such as state preparation flaws (SPFs), side-channels, Trojan horse attacks (THAs), and state correlations, can be estimated to guarantee the security of the actual QKD protocol [43].

Here, we propose a four-phase (FP) TFQKD protocol using coherent light sources and adopt the RT method to prove its practical security against all possible source flaws, including pulse correlations. The setup of TFQKD guarantees security against untrusted measurement devices. In addition, we demonstrate a proof-of-principle experimental implementation of our protocol to demonstrate its feasibility. Specifically, we fully characterize imperfect sources and introduce bounded fidelity to offer a secure key rate by using the RT method. Although bounded fidelity was first introduced in the Gottesman-Lo-Lütkenhaus-Preiskill (GLLP) analysis [45, 46], the

\* These authors contributed equally to this work

† hlyin@nju.edu.cn

‡ zbchen@nju.edu.cn

TABLE I. **Comparison of the experimental performance for different methods for QKD against source and detection flaws.** Ref. [44] is a side-channel-free QKD experiment (assuming perfect vacuum and without considering pulse correlations), and Refs. [13–15] present three recent experiments on DI-QKD.

	Distance (loss)	Key rate
This study	10 dB	108 kbps
	20 dB	1.63 kbps
Side-channel-free QKD [44]	50 km fiber (10.2 dB)	7.20 bps
DI-QKD [13]	2 m (3.5 m fiber)	$\sim 7.43$ bps
DI-QKD [14]	400 m (700 m fiber)	$8.54 \times 10^{-4}$ bps
DI-QKD [15]	220 m fiber	2.60 bps

GLLP analysis can be included under the RT method as a special case [42]. We simulated the secure key rate of our protocol and compared it with protocols in Ref. [43] and Ref. [39] against source flaws. The simulation results show that both in the ideal scenario and in the scenario with source flaws, the secure key rate of our protocol shows a higher performance than the other two protocols.

We specify the parameters characterizing source flaws and further relate them to data that can be measured experimentally to help generate a secure key rate in the experiment. Our experimental implementation only requires four-phase (quadrature phase-shift keying [47]) modulation of coherent states, which avoids intensity modulation correlation [48] and does not require vacuum state preparation. In addition, we conducted a finite-key analysis of our protocol. Considering source flaws, our experiments can achieve a key rate of 1.63 kbps with a 20 dB channel loss, which is a considerable progress compared with previous experimental implementations of QKD protocols with imperfect source and measurement devices [13–15, 44]. Our work is the first experimental implementation of a QKD protocol using the RT method [35, 42], with practical security against all possible imperfections in devices. The method we used to build relations between parameters estimated through the RT method and experimental data is also compatible with other potential source imperfections. Our study proves the feasibility of a practical secure QKD using the RT method. The features of our protocol also jointly show possible practicality for the future deployment of secure QKD systems with imperfect devices.

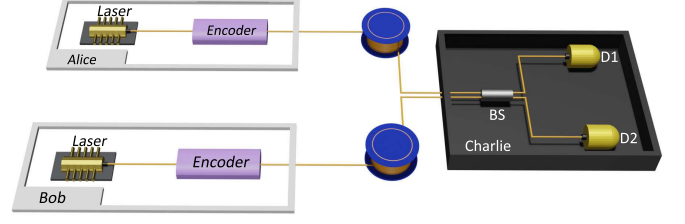


FIG. 1. **Schematic of our FP-TFQKD protocol.** At Alice's (Bob's) site, the simplified transmitter contains a laser source and an encoder. The encoder modulates the phase of the optical pulses. The modulation information of the encoder should be monitored to characterize the deviation between ideal and realistic pulses. If the untrusted Charlie is honest, he measures the signals received using an interference measurement.

## II. RESULTS

A brief schematic of the FP-TFQKD protocol is shown in Fig. 1. In our QKD system, Alice and Bob send weak coherent state pulses to an untrusted node, Charlie, who performs the interference measurement. For simplicity, we first describe our protocol under the assumption that Alice and Bob are able to prepare perfect optical pulses. Source flaws are thoroughly discussed. The protocol comprises the following steps:

(i) *Preparation.* In each turn, Alice randomly chooses the X and Y bases with probabilities  $p_x$  and  $p_y = 1 - p_x$ , respectively. If selecting the X basis, she picks a 'key' bit  $k_x^a \in \{0, 1\}$  and generates a weak coherent state pulse  $|e^{ik_x^a \pi} \alpha\rangle$ , where  $|\alpha|^2$  is the intensity of the optical pulse. When choosing the Y basis, she prepares a weak coherent state pulse  $|e^{i(k_y^a + \frac{1}{2})\pi} \alpha\rangle$  according to random bit  $k_y^a \in \{0, 1\}$ . Bob does the same.

(ii) *Measurement.* Alice and Bob send their optical pulses to an untrusted middle node Charlie through insecure quantum channels. Charlie is expected to perform interference measurements and record the detector that clicks.

Note that Charlie is assumed to apply a 50:50 beam splitter to the incoming two optical pulses, followed by two threshold single-photon detectors, D1 and D2. We assume that D1 (D2) will click when the phase difference between the two incoming optical pulses is zero ( $\pi$ ). We assume that Charlie records the situation when one and only one detector clicks as an effective measurement, regardless of the actual clicking results, because Charlie is an untrusted node and his betrayal can be included in the security analysis.

(iii) *Sifting.* Alice and Bob repeat Steps (i)–(ii) many times. Then, Charlie announces the effective measurements and detection results (whether D1 or D2 clicks). Alice and Bob maintain their corresponding keys and basis choices based on Charlie's announcement. If Charlie claims that D2 clicks, Bob will flip his key bit. Alice and

Bob then disclose their basis choices for effective measurements through authenticated classical channels, and further classify their key bits with basis information.

(iv) *Parameter estimation.* For the retained key bits in the X and Y bases, Alice and Bob obtain the gain. Then, they disclose all key bits under the Y basis to calculate the bit error rate, which is used to set a bound on the phase error rate.

(v) *Key distillation.* Alice and Bob perform error correction and privacy amplification on the remaining sifted keys under the X basis to distill the final secure key bits.

Evidently, the use of weak coherent state pulses naturally makes it easier for us to characterize the SPFs because any deviation in intensity and phase modulation between ideal pulses and realistic pulses can be directly shown in the expression of laser pulses. No assumptions on the Hilbert space dimensions are required. Our protocol further inherits the advantages that the QKD system can be implemented with fixed intensity because recent work reveals that intensity modulation introduces extra pulse correlations of intensity [48].

### A. Key rate of FP-TFQKD

As depicted in Fig. 1, the setting of two bases can introduce bounded fidelity with imbalance  $\Delta$  of a quantum coin [45]. For simplicity, we only present the main result for key rate estimation because the idea of a quantum coin has been discussed in previous works [45, 46] (see Supplementary Materials). Because only key bits under the X basis are used to form secure key bits, the final key rate of our FP-TFQKD protocol is given by

$$R = Q^x [1 - fH(E_b^x) - H(E_p)] \quad (1)$$

where  $Q^x$  denotes the gain under the X-basis.  $E_p$  is the phase error rate under the X-basis.  $E_b^x$  represents the quantum bit error rate under the X basis.  $H(x) = -x \log_2 x - (1-x) \log_2 (1-x)$  is the binary Shannon entropy function. According to the GLLP analysis and the RT method [42, 45, 46], the phase error rate  $E_p$  can be bounded by

$$1 - 2\Delta \leq \sqrt{E_b^y E_p} + \sqrt{(1 - E_b^y)(1 - E_p)}, \quad (2)$$

where  $E_b^y$  is the quantum bit error rate in the Y basis and  $\Delta$  quantifies the imbalance of Alice's and Bob's quantum coins based on their basis choices.  $\Delta$  can be bounded by the fidelity of the two basis-dependent states under the X and Y bases, which is denoted as  $|\langle \Psi_Y | \Psi_X \rangle|$ . In the symmetric scenario in which Alice and Bob share basis-dependent states, the simplified relation between  $\Delta$  and fidelity is  $1 - 2Q\Delta = |\langle \Psi_Y | \Psi_X \rangle|^2$ , where  $Q$  is the total gain (see Supplementary Materials). For the experimental implementation, the calculation of fidelity

with imperfect sources can be expressed as

$$\begin{aligned} \langle \Psi_X | \Psi_Y \rangle = & \frac{1}{4} (1 - \epsilon) e^{-\mu} \cos^2 \theta [(1 - i) \langle \alpha' | i e^{i\delta} \alpha' \rangle \\ & + (1 - i) \langle -e^{i\delta} \alpha' | -i e^{i\delta} \alpha' \rangle \\ & + (1 + i) \langle \alpha' | -i e^{i\delta} \alpha' \rangle \\ & + (1 + i) \langle -e^{i\delta} \alpha' | i e^{i\delta} \alpha' \rangle], \end{aligned} \quad (3)$$

where we use  $\epsilon$ ,  $\mu$ , and  $\theta$  to characterize the state correlations, THAs, and side channels, respectively. Here, we consider special cases of THAs and side channels as discussed in [35]. For the THAs,  $\mu$  is the intensity of the back-reflected light sent by the eavesdroppers. For the side channels,  $\theta$  is the parameter used to bound the side channels in the polarization space of our protocol in Eq. (9). Note that other potential side channels can also be characterized by additional parameters. For SPFs, we consider only the worst scenario with the maximum deviation in intensity and phase modulation without state correlations.  $|\alpha'|^2$  represents the realistic intensity modulation of coherent pulses, and the maximum deviation can be denoted by  $\xi$  and  $\xi = ||\alpha'|^2 - |\alpha|^2| / |\alpha|^2$ .  $\delta$  represents the deviation from the ideal phase modulation. Aside from the THAs, the parameters of the side channels and SPFs discussed here can be directly measured in the experiment, which can be seen in our experimental implementation. However, in experimental implementations, state correlations are usually measured in the form of a pattern effect [49], which means that  $\epsilon$  cannot be derived through experimental measurements. Our protocol was a FP-TFQKD with fixed intensity. The pattern effect occurs in the phase modulation, which is denoted as  $\psi$ , to represent the maximum deviation of the phase modulation caused by state correlations. Here, we derive a formula that relates the state correlation parameter  $\epsilon$  to the pattern effect  $\psi$ , which can be obtained as

$$\epsilon = 1 - e^{|\alpha|^2(2\cos\psi - 2)}. \quad (4)$$

Detailed calculations can be found in the Materials and Methods.

For experimental implementation, we provide a finite-key analysis of our protocol based on the method introduced in Ref. [50] and the analysis is secure against collective attacks. The formula for the number of secure key bits  $l$  can be expressed as

$$\begin{aligned} l = n_x \left[ 1 - H(\bar{E}_p) - \text{leak}_{\text{EC}} - 7 \sqrt{\frac{\log_2(2/\bar{\epsilon})}{n_x}} \right. \\ \left. - \frac{1}{n_x} \log_2 \frac{2}{\epsilon_{\text{EC}}} - \frac{2}{n_x} \log_2 \frac{1}{\epsilon_{\text{PA}}} \right], \end{aligned} \quad (5)$$

where  $n_x$  denotes the number of raw bits under the X basis, which is used to generate the secret key, and  $\text{leak}_{\text{EC}} = fH(E_b^x)$  represents the percentage of bits consumed during the procedure error correction.  $\epsilon_{\text{EC}}$  and

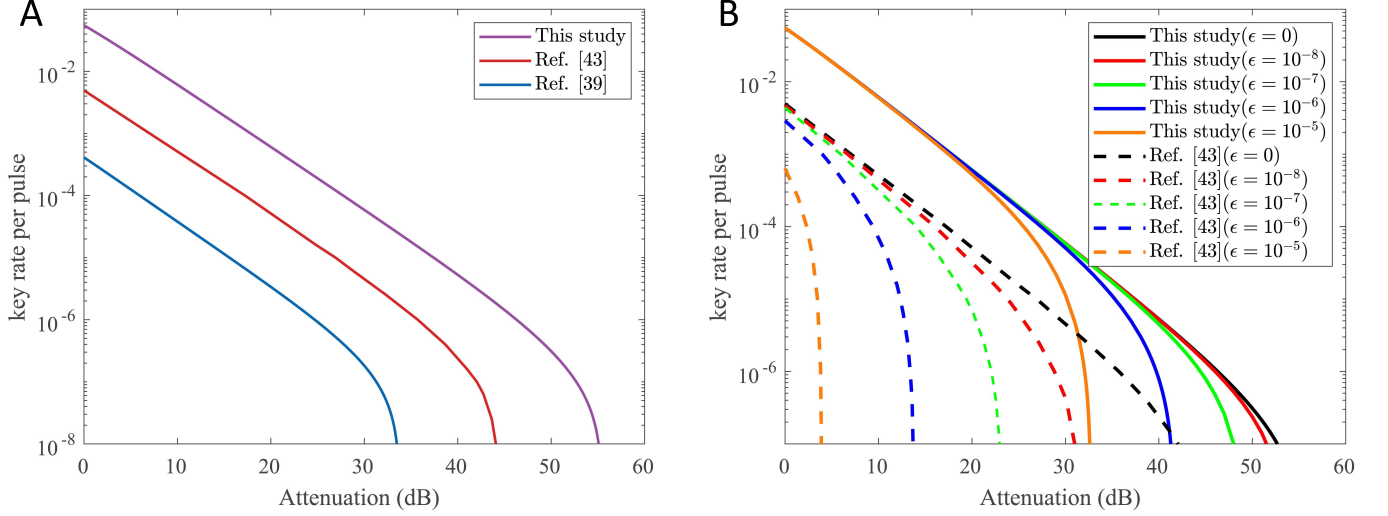


FIG. 2. **Key rate vs. the overall transmission loss.** (A) When there are no source flaws, we compare the performance of our protocol (violet line) with that of two other protocols in Ref. [43] (red line) and Ref. [39] (blue line). An evident improvement in the key rate indicates that our protocol outperformed the other two protocols. (B) We applied the same parameter  $\epsilon$  as in Ref. [43] to characterize general side channels and depict the performance of secret key rates in both our protocol and the protocol in Ref. [43] for different values of  $\epsilon$  ( $0, 10^{-8}, 10^{-7}, 10^{-6}, 10^{-5}$ ) using different colors. Evidently, our protocol (solid lines) outperforms the protocol described in Ref. [43] (dashed lines) with respect to key rate. With  $\epsilon = 10^{-5}$ , the orange solid line can still generate a secure key rate when the total loss is 30 dB, whereas the orange dashed line can barely generate a secure key rate.

$\epsilon_P A$  represent the failure probabilities for the error correction and privacy amplification, respectively.  $\bar{\epsilon}$  is the other error probability that measures the accuracy of estimating smooth min-entropy. In addition, statistical fluctuations should be applied to determine the upper bound of the observed phase-error rate  $\bar{E}_p$ . Detailed formulas can be found in the Supplementary Materials, with bounds introduced in Ref. [51, 52]. Although we only offer finite-key analysis against collective attacks here, there have been studies demonstrating how to improve the security of finite-key analysis to resist coherent attacks [53, 54].

## B. Simulation results

To evaluate the performance of our protocol theoretically, we simulate the secure key rates of our protocol in two different scenarios, sharing one precondition that we only conduct simulations in the asymptotic scenario. Specifically, we set the detector efficiency  $\eta_d = 1$  and the dark count rate  $p_d = 10^{-8}$ . The error correction efficiency  $f$  in Eq. (1), and Eq. (S8) was set to 1.16. The simulation results are shown in Fig. 2, respectively.

In the first scenario, shown in Fig. 2A, we only considered the ideal scenario with no source flaws, which means that the parameters characterizing the source flaws can easily be set to zero. For comparison, we also depict the key rates of the two other side-channel-free protocols in Ref. [43], and Ref. [39]). The simulation results clearly illustrate that, when the total attenuation approaches 50

dB, only our protocol can generate secret keys. With the same transmission loss, the key rate of our protocol was approximately one order of magnitude higher than that of the protocol in Ref. [43], and approximately two orders of magnitude higher than that of the protocol in Ref. [39]).

In the second scenario, as illustrated in Fig. 2B, we analyzed the security of our protocol compared to that in Ref. [43], which generalizes all the side channels to a single parameter,  $\epsilon$ . From the formula for the practical secure key rate in Eq. (13), if we only consider the state correlation flaws and set the other parameters to zero,  $\epsilon$  can be converted into the parameter introduced in Ref. [43], which characterizes general side-channels. Based on this, we evaluated the key rate of our protocol for different degrees of general side channels ( $\epsilon = 0, 10^{-8}, 10^{-7}, 10^{-6}, 10^{-5}$ ). In Fig. 2B, when  $\epsilon$  increases, a decrease in the key rate can be observed both in our study and in the protocol in Ref. [43], and a better performance can be observed in our secret key rate with the same  $\epsilon$ . Additionally, our protocol can still generate a considerable secret key rate when  $\epsilon = 10^{-5}$ .

## C. Experimental implementation

Here, we present a proof-of-principle experimental demonstration of the FP-TFQKD protocol. The setup is illustrated in Fig. 3). This is a plug-and-play construction consisting of a Sagnac interferometer, similar to the



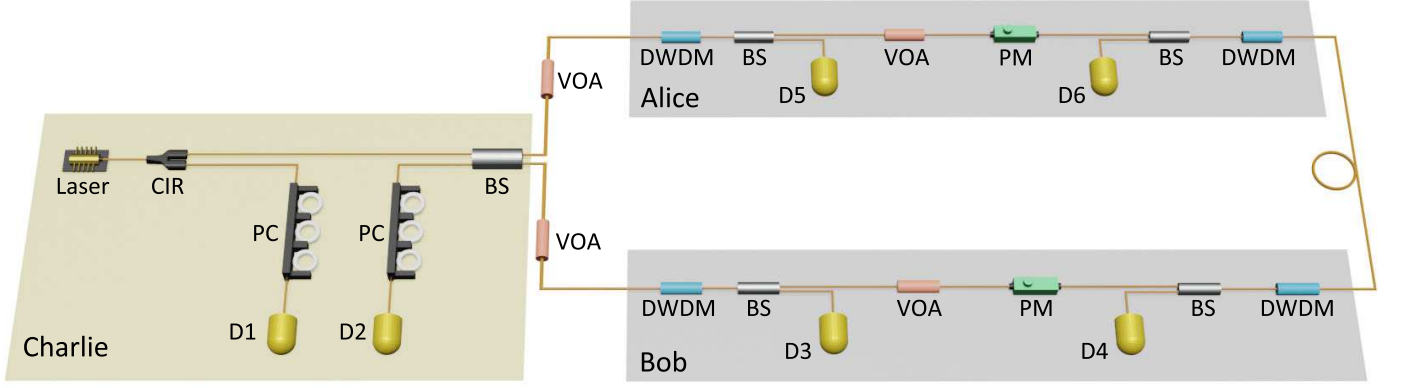


FIG. 3. **Experimental setup of our plug-and-play system.** Optical pulses are directly generated by a pulsed laser source and then passed through a circulator (CIR). These pulses are separated into two pulse sequences with different propagation directions using a 50 : 50 beam splitter (BS). The clockwise pulse sequence is modulated by a phase modulator (PM) controlled by an arbitrary waveform generator after passing dense wavelength division multiplexing (DWDM) and a BS. A counterclockwise pulse sequence undergoes a similar process. Finally, these two pulses interfere in the BS and are detected by two superconducting nanowire single-photon detectors D1 and D2. Polarization controllers (PC) are used to modify the polarization of the incident pulses to achieve maximum detection efficiencies.

system in Ref. [55, 56]. We use the Sagnac loop to stabilize the phase fluctuation of the channel automatically, and all optical fibers maintain polarization.

Optical pulses are generated using a homemade pulsed laser. Pulses with a frequency of 100 MHz have an extinction ratio greater than 30 dB and a pulse width of less than 300 ps. Charlie sends the optical pulses to Alice and Bob. These optical pulses pass through a circulator and are then separated by a 50:50 BS into two identical pulses. The two pulses are phase modulated by Alice and Bob. Specifically, clockwise (counterclockwise) pulses are modulated by Alice (Bob). In addition, four DWDMs are used for the bandpass filter, and four BSs are utilized to monitor the intensity of pulses entering Alice's or Bob's site, with the aim of protecting against attacks from injected pulses. In fact, we did not monitor the intensity and filter pulses during implementation because of resource limitations, which should be addressed for security. However, these processes can be directly added to our system with little influence on the results. Alice (Bob) chooses the X basis with a probability of  $p_x = 90\%$  and the Y basis with a probability of  $p_y = 10\%$ . The radio frequency signals for modulation and clock signals of the experimental system are produced by an arbitrary waveform generator (Tabor Electronics, P2588B).

After the phase modulations, Alice (Bob) send pulses through a variable optical attenuator before the Charlie's beam splitter. The loss between Alice (Bob) and Charlie is adjusted to simulate the loss of the communication channel. Pulses from Alice and Bob interfere at the BS. One output of this BS is detected by a single-photon detector D1 via the circulator, whereas the other output is followed directly by D2. The dark count rates were  $1.6 \times 10^{-8}$  and  $2.5 \times 10^{-8}$  (1.5 ns per time window), respectively. The relevant system parameters are listed

TABLE II. **Experimental parameters in the FP-TFQKD system.** The experimental parameters include the laser wavelength  $\lambda$ , total efficiencies of the optical elements at the detection site,  $\eta_{\text{det1}}$  and  $\eta_{\text{det2}}$ , and detection efficiencies of the two detectors,  $\eta_{\text{D1}}$  and  $\eta_{\text{D2}}$ .  $\eta_{\text{det1}}$  consists of the efficiencies of three main components: the beam splitter, circulator, and polarization controller, whereas  $\eta_{\text{det2}}$  includes the beam splitter and polarization controller.

$\lambda$	$\eta_{\text{det1}}$	$\eta_{\text{det2}}$	$\eta_{\text{D1}}$	$\eta_{\text{D2}}$
1550.14 nm	75.3%	83.6%	88.0%	85.5%

in Table II.

We measured and quantified four types of source flaws in this system: imperfect intensity modulation, imperfect phase modulation, polarization contrast (side channels), and pattern effects (state correlation). It should be noted that THAs cannot be quantified in this implementation, and we set them to 0. Imperfect intensity modulation is quantified by the intensity fluctuation  $\xi$  of the pulses sent, because there is no intensity modulation in this protocol. Imperfect phase modulation can be quantitatively characterized by the difference  $\delta$  between the actual and expected phases. For polarization contrast (side-channels), we measured the polarization contrast  $\tan\theta$  of the pulses sent when the system was running. The pattern effects (state correlation) were quantified by the interference results of the same phases under different patterns and 0 phase, which is denoted as  $\psi$ . The results are presented in Table III, and all parameters correspond to those introduced in Eq. (3). Detailed descriptions of the derivation of these parameters are provided in Supplementary Materials.

To demonstrate the advantages of our protocol when

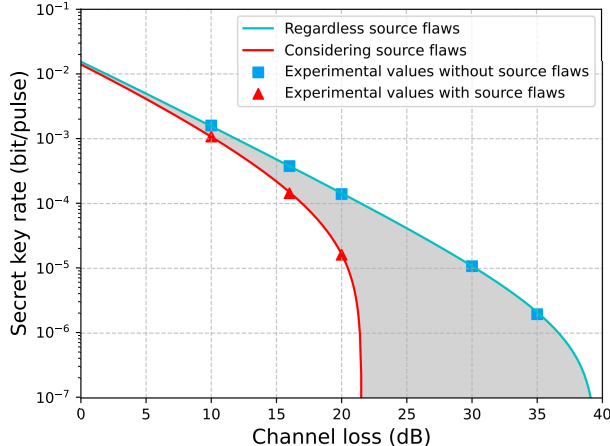


FIG. 4. **Secret key rate (per pulse) vs. the channel loss between Alice and Bob with  $N = 10^{10}$ .** The filled symbols indicate the experimental results obtained for whether source flaws were considered. The solid lines correspond to the theoretical simulation results for our protocol, under different assumptions.

considering source flaws, we implemented experiments under three values of channel losses between Alice and Bob: 10 dB, 16 dB, and 20 dB, as shown in Fig. 4. We further performed experiments under channel losses of 30 dB and 35 dB, with the assumption that the sources are perfect. The shaded area between the blue and red lines shown in Fig. 4 is unsafe and need to be considered seriously. The blue line can be reached by rigorously narrowing the parameters in Table. III to approximately 0. Considering imperfect sources, our protocol can obtain secure key bits when the channel loss is over 20 dB, which means that it can be implemented over 100 km using existing technologies. The key rate of 1.63 kbps we achieved under a channel loss of 20 dB is the best result for the transmission distance and key rate considering both source and detection imperfections. Under 10 dB ( $\sim 50$  km), the key rate of our protocol is over 100 kbps, whereas under 16 dB ( $\sim 80$  km), the key rate is over 10 kbps. Furthermore, if we set the parameter of THAs to  $\mu = 10^{-7}$  [57], the key rate drops by 1.9% under 20 dB. Regardless of the source flaws, we achieved a key rate of 196 bps with a channel loss of 35 dB. Detailed experimental results are presented in Table. IV. Although we cannot actually demonstrate THAs in our experiment, a recent work focused on resisting THAs, and its creative design of optical power limiters can also be applied in our work against THAs [58]. In addition, despite the fact that optical fibers were not used in the actual implementation and the two users were not separated, as a proof-of-principle demonstration, we focused on the feasibility of our protocol rather than aiming to establish a complete system with all necessary hardware. Combined with the developed phase-locking and phase-

TABLE III. **Five parameters related to the imperfection of realistic sources.** The parameters included the intensity fluctuation  $\xi$ , polarization contrast  $\tan\theta$ , phase shift  $\delta$ , pattern effect  $\psi$ , and THAs  $\mu$ .

$\xi$	$\tan\theta$	$\delta$	$\psi$	$\mu$
1.17%	$10^{-2.65}$	0.062	$8.54 \times 10^{-3}$	0

tracking technology in the implementation of twin-field QKD [27–31], our protocol containing two independent users can be directly implemented in real optical fibers, which is illustrated in detail in the Supplementary Materials.

### III. DISCUSSION

Based on the fact that tremendous progress has been witnessed in the deployment of QKD, practical secure QKD protocols are becoming an important research direction in quantum communication since they are relevant for the practical deployment of QKD. In this study, we propose an FP-TFQKD protocol using coherent states that can be guaranteed to be secure against realistic flawed sources. We further demonstrate the feasibility of the protocol through a proof-of-principle experimental implementation [18]. By combining the twin-field setup and security analysis with the RT method, the practical security of our protocol against device imperfections can be proven. For source flaws, we consider SPFs, side channels, THAs, and state correlations, which typically cover all possible source imperfections that are currently observed in experimental implementations. Although we only consider the special polarization side-channel and one special THA, we note that other side-channels and THAs can also be included in the calculation of fidelity with extra parameters. In addition, we offer relations between parameters characterizing source flaws and experimental data, and provide specific implementations in our experiment on how to define and measure these parameters, which can be applied to other types of source flaws. Therefore, our protocol is more practical than other QKD protocols considering imperfect devices. In addition, the simulation results show that our protocol generates a higher secure key rate against source flaws than the other QKD protocols in Ref. [43] and Ref. [39]). In particular, compared to the side-channel-free QKD in Ref. [39], and its experimental implementation in Ref. [44], our work removes the requirement of vacuum state preparation, which introduces intensity correlations that invalidate the key assumption of this method [48]. For experimental implementation, we also present a finite-key analysis against collective attacks, and the method we use can be easily modified to prove security against coherent attacks [53, 54].

Furthermore, we experimentally demonstrate our pro-

TABLE IV. **Summary of experimental data.** We tested the key rates for different channel losses. The table shows the number of pulses sent, the expected intensity of pulses  $\mu' = |\alpha|^2$ , the number of detection events under corresponding bases, the experimental quantum bit error rates under the X basis and Y basis, the number of clicks under the X basis  $S_X^L$ , the key rate  $R^*$  regardless of source flaws, and the key rate  $R$  considering source flaws.

Loss	$N$	$\mu'$	$E_b^X$	$E_b^Y$	$S_X^L$	$R^*$	$R$
10 dB	$10^{10}$	$1.38 \times 10^{-2}$	0.23%	0.36%	49398692	$1.60 \times 10^{-3}$	$1.08 \times 10^{-3}$
16 dB	$10^{10}$	$5.70 \times 10^{-3}$	0.23%	0.38%	11421107	$3.78 \times 10^{-4}$	$1.44 \times 10^{-4}$
20 dB	$10^{10}$	$3.30 \times 10^{-3}$	0.22%	0.36%	3718173	$1.40 \times 10^{-4}$	$1.63 \times 10^{-5}$
30 dB	$10^{10}$	$1.31 \times 10^{-3}$	0.27%	0.42%	464991	$1.08 \times 10^{-5}$	0
35 dB	$10^{10}$	$6.27 \times 10^{-4}$	0.33%	0.57%	124117	$1.96 \times 10^{-6}$	0

tol using a plug-and-play system. With perfect sources, our protocol can be demonstrated over 35 dB, which is a considerable improvement in the transmission distance in the realm of practical secure QKD. By removing assumptions of the perfect source and detection site, our protocol can still achieve a key rate of 1.63 kbps with a 20 dB channel loss, which outperforms other experimental implementations of practical secure QKD protocols. Besides, we also achieve key rates of 108 kbps and 14.4 kbps at 10 dB and 16 dB, respectively. The transmission distance of our protocol was constrained using five parameters relevant to imperfect sources. However, these five parameters can be optimized; thus, the key rate and transmission distance of this protocol can be further improved. First, the measurements of these parameters are limited by the accuracy and precision of the devices. For example, the accuracy of the power meter measuring intensity fluctuations is limited, and the power meter itself has jitters, which may result in larger fluctuations. Additionally, the values of these parameters can be further reduced using available technologies. More accurate phase modulation can be achieved by using more phase modulators, which can avoid nonlinear amplification of radio frequency signals. The polarization contrast can be further improved by fusing optical fibers or by adding a polarizer at the user's site. With developed technologies, these parameters will be closer to 0. Note that our scheme does not need to resort to immature technologies such as entanglement or single-photon sources, which makes our scheme practical. Overall, our work further proves the feasibility of secure QKD with arbitrary flawed devices, and holds the potential to be applied to the future deployment of practical secure QKD.

#### IV. MATERIALS AND METHODS

##### A. Source flaws

We characterized the expression for basis-dependent states using our protocol. First, an ideal scenario is presented. Then, we discuss how to jointly consider different realistic source flaws (SPFs, side-channels, THAs and

state correlations) to describe the basis-dependent states.

##### 1. The ideal scenario

In an ideal scenario, Alice and Bob prepare perfect weakly coherent states. The symmetric scenario is another assumption under which the states Alice and Bob prepare are the same. The basis-dependent states are

$$\begin{aligned} |\Psi_X\rangle &= \frac{1}{\sqrt{2}} (|0_X\rangle |\alpha\rangle + |1_X\rangle |-\alpha\rangle), \\ |\Psi_Y\rangle &= \frac{1}{\sqrt{2}} (|1_Y\rangle |i\alpha\rangle + |0_Y\rangle |-i\alpha\rangle), \end{aligned} \quad (6)$$

where  $\{|0_X\rangle, |1_X\rangle\}$  and  $\{|0_Y\rangle, |1_Y\rangle\}$  are the eigenstates of the Pauli operators  $\sigma_x$  and  $\sigma_y$ , respectively. Then, we obtain the joint-bounded fidelity as

$$|\langle \Psi_X | \Psi_Y \rangle|^2 = e^{-2|\alpha|^2} [1 + \sin(2|\alpha|^2)]. \quad (7)$$

##### 2. The realistic scenario

**State preparation flaws.** When considering SPFs in practical implementations, there is an inherent advantage of using weak coherent pulses as SPFs can be characterized by imperfect intensity and phase modulations on weak coherent pulses. The actual basis-dependent states with SPFs can be expressed as

$$\begin{aligned} |\Psi_X\rangle^* &= \frac{1}{\sqrt{2}} (|0_X\rangle |\alpha_0\rangle + |1_X\rangle |-e^{i\delta_1}\alpha_1\rangle), \\ |\Psi_Y\rangle^* &= \frac{1}{\sqrt{2}} (|1_Y\rangle |ie^{i\delta_2}\alpha_2\rangle + |0_Y\rangle |-ie^{i\delta_3}\alpha_3\rangle). \end{aligned} \quad (8)$$

Note that the phase in  $|\alpha_0\rangle$  can be regarded as the global phase and does not affect the bounded fidelity of the two bases. Here, we consider a situation with varied basis and bit choices, which have different deviations of intensity and phase modulations, to derive the general expression of the basis-dependent states. For the simulation and

experimental implementations, as mentioned before, we only considered the worst scenario with maximum deviations in intensity and phase modulations without state correlations.

**Side channels.** Side channels are common imperfections in a practical QKD system, where the eavesdropper Eve can exploit dimensions other than the encoding dimension to distinguish states that carry the secret. For example, in our protocol, the bits are encoded in phase space, which is the operational space, and Eve can distinguish signals from senders using the polarization information of each state, which is one of the side channels. Here, we consider only the polarization space as the side-channel space, together with a polarization multimode scenario. We express the weak coherent states according to the basis and bit information as follows:

$$\begin{aligned} |\alpha'_0\rangle &= \cos\theta_0 |\alpha_0\rangle_H + \sin\theta_0 |\alpha_0\rangle_V, \\ |\alpha'_1\rangle &= \cos\theta_1 |-e^{i\delta_1}\alpha_1\rangle_H + \sin\theta_1 |-e^{i\delta_1}\alpha_1\rangle_V, \\ |\alpha'_2\rangle &= \cos\theta_2 |ie^{i\delta_2}\alpha_2\rangle_H + \sin\theta_2 |ie^{i\delta_2}\alpha_2\rangle_V, \\ |\alpha'_3\rangle &= \cos\theta_3 |-ie^{i\delta_3}\alpha_3\rangle_H + \sin\theta_3 |-ie^{i\delta_3}\alpha_3\rangle_V, \end{aligned} \quad (9)$$

where H and V refer to the horizontal and vertical polarization modes, respectively. In addition, we assume that  $\theta_0 = \theta_1 = \theta_2 = \theta_3 = \theta$ , as we consider the worst situation when the maximum deviation of polarization  $\theta$  occurs for every state. We adopt only states in the horizontal polarization mode to form the secure key rate, and  $\theta$  can be directly measured through the polarization contrast. We obtain the basis-dependent states with side channels and SPFs as

$$\begin{aligned} |\Psi_X\rangle' &= \frac{1}{\sqrt{2}} (|0_X\rangle |\alpha'_0\rangle + |1_X\rangle |\alpha'_1\rangle), \\ |\Psi_Y\rangle' &= \frac{1}{\sqrt{2}} (|1_Y\rangle |\alpha'_2\rangle + |0_Y\rangle |\alpha'_3\rangle). \end{aligned} \quad (10)$$

**Trojan horse attacks.** THAs have been recognized as powerful eavesdropping strategies [57, 58]. Here, we consider a special THA in which Eve can inject strong light into Alice's and Bob's sites through the quantum channel and obtain the phase modulation information by measuring the light reflected from Alice's and Bob's optical devices. Here, we can assume that the back-reflected strong light Eve sends to Alice's (Bob's) site is a strong coherent pulse:

$$|\zeta_T\rangle_E = e^{-\mu/2} |v_T\rangle_E + \sqrt{1 - e^{-\mu}} |\xi_T\rangle_E, \quad (11)$$

where  $T \in \{0X, 0Y, 1X, 1Y\}$  denotes the bit and basis choices of Alice and Bob and  $\mu$  is the intensity of Eve's back-reflected light. Here, we apply the model of THAs, in which  $|\zeta_T\rangle_E$  is a coherent state and  $|v_T\rangle_E$  is the vacuum state [35]. For simplicity, we consider the worst scenario in which the overlap is  $\langle \xi_T | \xi_{T'} \rangle_E = 0$ . When jointly

considering the SPFs and side-channel effects, the basis-dependent states can be written as

$$\begin{aligned} |\Psi_X\rangle'' &= \frac{1}{\sqrt{2}} (|0_X\rangle |\alpha'_0\rangle |\zeta_{0X}\rangle_E + |1_X\rangle |\alpha'_1\rangle |\zeta_{1X}\rangle_E), \\ |\Psi_Y\rangle'' &= \frac{1}{\sqrt{2}} (|1_Y\rangle |\alpha'_2\rangle |\zeta_{1Y}\rangle_E + |0_Y\rangle |\alpha'_3\rangle |\zeta_{0Y}\rangle_E). \end{aligned} \quad (12)$$

**State correlations.** State correlation is another security loop hole in a practical QKD system [42, 48, 49, 59], which is caused by different modulations between coherent pulses and can reveal the modulation information to Eve. Because vacuum state modulation is avoided in this study, it is not necessary to consider the intensity correlation between pulses [48]. However, in our protocol, phase modulation also introduces state correlations, which is observed in our experiments. Fortunately, it has been theoretically demonstrated that state correlations can be interpreted as side channel effects [42]. We can obtain the state-dependent states as

$$\begin{aligned} |\Psi_X\rangle &= \sqrt{1 - \epsilon} |\Psi_X\rangle'' + \sqrt{\epsilon} |\Psi_X^\perp\rangle, \\ |\Psi_Y\rangle &= \sqrt{1 - \epsilon} |\Psi_Y\rangle'' + \sqrt{\epsilon} |\Psi_Y^\perp\rangle, \end{aligned} \quad (13)$$

where  $\epsilon$  is a parameter characterizing the state correlations in the phase modulations, and the specific expression of  $|\Psi_{X(Y)}^\perp\rangle$  can be ignored, together with the worst situation for the senders, where  $\langle \Psi_X^\perp | \Psi_Y^\perp \rangle = 0$ . However, in the experiment, we could only measure the deviation of phase modulations caused by state correlations, which is referred to as the pattern effect [49]. Here, we only recorded the maximum phase deviation, which is denoted as  $\psi$ . Then, we derived the relationship between the abstract parameter  $\epsilon$  and the pattern effect  $\psi$ . For simplicity, our discussion is based on the condition that imperfections other than the state correlations are neglected. For example, when the ideal state without any imperfection is  $|\alpha\rangle$ , corresponding to bit 1 on the X basis, the phase modulations of other states will be influenced by state correlations owing to the phase modulation of  $|\alpha\rangle$ . The practical state corresponds to  $|-e^{i\psi}\alpha\rangle$ . Similar to the basic idea for finding the reference state, we can write the practical state as

$$|-e^{i\psi}\alpha\rangle = e^{(e^{i\psi}-1)|\alpha|^2} |\alpha\rangle + \sqrt{1 - e^{2(e^{i\psi}-1)|\alpha|^2}} |-\alpha^\perp\rangle, \quad (14)$$

where  $\langle -\alpha | -e^{i\psi}\alpha \rangle = e^{(e^{i\psi}-1)|\alpha|^2}$  and there is no need to write down the specific expression of  $|\alpha^\perp\rangle$ . The definition of  $\epsilon$  leads to the formula  $\sqrt{1 - \epsilon} = e^{(e^{i\psi}-1)|\alpha|^2}$ , and we obtain the relation  $\epsilon = 1 - e^{|\alpha|^2(2\cos\psi-2)}$ . For other bit and basis choices, it is readily observed that the formula remains the same.

## B. The calculation of the basis-dependent states

Here, we need to calculate the analytic formula for the bounded fidelity to estimate the imbalance  $\Delta$ . The



fidelity  $\langle \Psi_X | \Psi_Y \rangle$  becomes  $\langle \Psi_X | \Psi_Y \rangle = (1 - \epsilon) \langle \Psi_X | \Psi_Y \rangle''$  and

$$\begin{aligned} \langle \Psi_X | \Psi_Y \rangle'' = & \frac{1}{4} e^{-\mu} \cos^2 \theta [(1 - i) \langle \alpha_0 | i e^{i\delta_2} \alpha_2 \rangle \\ & + (1 - i) \langle -e^{i\delta_1} \alpha_1 | -i e^{i\delta_3} \alpha_3 \rangle \\ & + (1 + i) \langle \alpha_0 | -i e^{i\delta_3} \alpha_3 \rangle \\ & + (1 + i) \langle -e^{i\delta_1} \alpha_1 | i e^{i\delta_2} \alpha_2 \rangle], \end{aligned} \quad (15)$$

which can be applied to the calculation of joint fidelity  $|\langle \Psi_Y | \Psi_X \rangle|^2$ . For simplicity, we further assumed that  $\delta_1 = \delta_2 = \delta_3 = \delta$  and  $\alpha_0 = \alpha_1 = \alpha_2 = \alpha_3 = \alpha'$ , which

represent the maximum deviations of the intensity and phase modulations, respectively, as shown in Eq. (3).

### Acknowledgments

We thank P.Liu and Y.-S.Lu for valuable discussion and Y.Bao and S.-C.Huang for experimental assistance. This study was supported by the Natural Science Foundation of Jiangsu Province (No. BK20211145), the Fundamental Research Funds for the Central Universities (No. 020414380182), the Key Research and Development Program of Nanjing Jiangbei New Area (No. ZDYD20210101), the Program for Innovative Talents, and Entrepreneurs in Jiangsu (No. JSSCRC2021484).

- 
- [1] C. H. Bennett and G. Brassard, Quantum cryptography: Public key distribution and coin tossing, *Theor. Comput. Sci.* **560**, 7 (2014).
  - [2] A. K. Ekert, Quantum cryptography based on bell's theorem, *Phys. Rev. Lett.* **67**, 661 (1991).
  - [3] F. Xu, X. Ma, Q. Zhang, H.-K. Lo, and J.-W. Pan, Secure quantum key distribution with realistic devices, *Rev. Mod. Phys.* **92**, 025002 (2020).
  - [4] S. Pirandola, U. L. Andersen, L. Banchi, M. Berta, D. Bunandar, R. Colbeck, D. Englund, T. Gehring, C. Lupo, C. Ottaviani, *et al.*, Advances in quantum cryptography, *Adv. Opt. Photonics* **12**, 1012 (2020).
  - [5] L. Lydersen, C. Wiechers, C. Wittmann, D. Elser, J. Skaar, and V. Makarov, Hacking commercial quantum cryptography systems by tailored bright illumination, *Nat. Photonics* **4**, 686 (2010).
  - [6] Y.-L. Tang, H.-L. Yin, X. Ma, C.-H. F. Fung, Y. Liu, H.-L. Yong, T.-Y. Chen, C.-Z. Peng, Z.-B. Chen, and J.-W. Pan, Source attack of decoy-state quantum key distribution using phase information, *Phys. Rev. A* **88**, 022308 (2013).
  - [7] F. Xu, B. Qi, and H.-K. Lo, Experimental demonstration of phase-remapping attack in a practical quantum key distribution system, *New J. Phys.* **12**, 113026 (2010).
  - [8] A. Huang, A. Navarrete, S.-H. Sun, P. Chaiwongkhot, M. Curty, and V. Makarov, Laser-seeding attack in quantum key distribution, *Phys. Rev. Applied* **12**, 064043 (2019).
  - [9] A. Acín, N. Brunner, N. Gisin, S. Massar, S. Pironio, and V. Scarani, Device-independent security of quantum cryptography against collective attacks, *Phys. Rev. Lett.* **98**, 230501 (2007).
  - [10] B. Hensen, H. Bernien, A. E. Dréau, A. Reiserer, N. Kalb, M. S. Blok, J. Ruitenberg, R. F. L. Vermeulen, R. N. Schouten, C. Abellán, W. Amaya, V. Pruneri, M. W. Mitchell, M. Markham, D. J. Twitchen, D. Elkouss, S. Wehner, T. H. Taminiau, and R. Hanson, Loophole-free bell inequality violation using electron spins separated by 1.3 kilometres, *Nature* **526**, 682 (2015).
  - [11] L. K. Shalm, E. Meyer-Scott, B. G. Christensen, P. Bierhorst, M. A. Wayne, M. J. Stevens, T. Gerrits, S. Glancy, D. R. Hamel, M. S. Allman, K. J. Coakley, S. D. Dyer, C. Hodge, A. E. Lita, V. B. Verma, C. Lambrocco, E. Tortorici, A. L. Migdall, Y. Zhang, D. R. Kumor, W. H. Farr, F. Marsili, M. D. Shaw, J. A. Stern, C. Abellán, W. Amaya, V. Pruneri, T. Jennewein, M. W. Mitchell, P. G. Kwiat, J. C. Bienfang, R. P. Mirin, E. Knill, and S. W. Nam, Strong loophole-free test of local realism, *Phys. Rev. Lett.* **115**, 250402 (2015).
  - [12] M. Giustina, M. A. M. Versteegh, S. Wengerowsky, J. Handsteiner, A. Hochrainer, K. Phelan, F. Steinlechner, J. Kofler, J.-A. Larsson, C. Abellán, W. Amaya, V. Pruneri, M. W. Mitchell, J. Beyer, T. Gerrits, A. E. Lita, L. K. Shalm, S. W. Nam, T. Scheidl, R. Ursin, B. Wittmann, and A. Zeilinger, Significant-loophole-free test of bell's theorem with entangled photons, *Phys. Rev. Lett.* **115**, 250401 (2015).
  - [13] D. Nadlinger, P. Drmota, B. Nichol, G. Araneda, D. Main, R. Srinivas, D. Lucas, C. Ballance, K. Ivanov, E. Tan, *et al.*, Device-independent quantum key distribution, *arXiv preprint arXiv:2109.14600* (2021).
  - [14] W. Zhang, T. van Leent, K. Redeker, R. Garthoff, R. Schwonnek, F. Fertig, S. Eppelt, V. Scarani, C. C.-W. Lim, and H. Weinfurter, Experimental device-independent quantum key distribution between distant users, *arXiv preprint arXiv:2110.00575* (2021).
  - [15] W.-Z. Liu, Y.-Z. Zhang, Y.-Z. Zhen, M.-H. Li, Y. Liu, J. Fan, F. Xu, Q. Zhang, and J.-W. Pan, High-speed device-independent quantum key distribution against collective attacks, *arXiv preprint arXiv:2110.01480* (2021).
  - [16] M. Farkas, M. Balanzó-Juandó, K. Łukanowski, J. Kołodyński, and A. Acín, Bell nonlocality is not sufficient for the security of standard device-independent quantum key distribution protocols, *Phys. Rev. Lett.* **127**, 050503 (2021).
  - [17] H.-K. Lo, M. Curty, and B. Qi, Measurement-device-independent quantum key distribution, *Phys. Rev. Lett.* **108**, 130503 (2012).
  - [18] M. Lucamarini, Z. L. Yuan, J. F. Dynes, and A. J. Shields, Overcoming the rate-distance limit of quantum key distribution without quantum repeaters, *Nature* **557**, 400 (2018).
  - [19] A. Rubenok, J. A. Slater, P. Chan, I. Lucio-Martinez, and W. Tittel, Real-world two-photon interference and proof-of-principle quantum key distribution immune to detector attacks, *Phys. Rev. Lett.* **111**, 130501 (2013).
  - [20] Y.-L. Tang, H.-L. Yin, S.-J. Chen, Y. Liu, W.-J. Zhang, X. Jiang, L. Zhang, J. Wang, L.-X. You, J.-Y. Guan, *et al.*, Measurement-device-independent quantum key

- distribution over 200 km, Phys. Rev. Lett. **113**, 190501 (2014).
- [21] C. Wang, X.-T. Song, Z.-Q. Yin, S. Wang, W. Chen, C.-M. Zhang, G.-C. Guo, and Z.-F. Han, Phase-reference-free experiment of measurement-device-independent quantum key distribution, Phys. Rev. Lett. **115**, 160502 (2015).
- [22] Y.-H. Zhou, Z.-W. Yu, and X.-B. Wang, Making the decoy-state measurement-device-independent quantum key distribution practically useful, Phys. Rev. A **93**, 042324 (2016).
- [23] Z. Tang, Z. Liao, F. Xu, B. Qi, L. Qian, and H.-K. Lo, Experimental demonstration of polarization encoding measurement-device-independent quantum key distribution, Phys. Rev. Lett. **112**, 190503 (2014).
- [24] L. C. Comandar, M. Lucamarini, B. Fröhlich, J. F. Dynes, A. W. Sharpe, S. W.-B. Tam, Z. L. Yuan, R. V. Penty, and A. J. Shields, Quantum key distribution without detector vulnerabilities using optically seeded lasers, Nat. Photonics **10**, 312 (2016).
- [25] X. Zheng, P. Zhang, R. Ge, L. Lu, G. He, Q. Chen, F. Qu, L. Zhang, X. Cai, Y. Lu, *et al.*, Heterogeneously integrated, superconducting silicon-photonics platform for measurement-device-independent quantum key distribution, Adv. Photonics **3**, 055002 (2021).
- [26] Y.-M. Xie, Y.-S. Lu, C.-X. Weng, X.-Y. Cao, Z.-Y. Jia, Y. Bao, Y. Wang, Y. Fu, H.-L. Yin, and Z.-B. Chen, Breaking the rate-loss bound of quantum key distribution with asynchronous two-photon interference, PRX Quantum **3**, 0203 (2022).
- [27] H.-L. Yin, T.-Y. Chen, Z.-W. Yu, H. Liu, L.-X. You, Y.-H. Zhou, S.-J. Chen, Y. Mao, M.-Q. Huang, W.-J. Zhang, H. Chen, M. J. Li, D. Nolan, F. Zhou, X. Jiang, Z. Wang, Q. Zhang, X.-B. Wang, and J.-W. Pan, Measurement-device-independent quantum key distribution over a 404 km optical fiber, Phys. Rev. Lett. **117**, 190501 (2016).
- [28] X.-T. Fang, P. Zeng, H. Liu, M. Zou, W. Wu, Y.-L. Tang, Y.-J. Sheng, Y. Xiang, W. Zhang, H. Li, Z. Wang, L. You, M.-J. Li, H. Chen, Y.-A. Chen, Q. Zhang, C.-Z. Peng, X. Ma, T.-Y. Chen, and J.-W. Pan, Implementation of quantum key distribution surpassing the linear rate-transmittance bound, Nat. Photonics **14**, 422 (2020).
- [29] M. Pittaluga, M. Minder, M. Lucamarini, M. Sanzaro, R. I. Woodward, M.-J. Li, Z. Yuan, and A. J. Shields, 600-km repeater-like quantum communications with dual-band stabilization, Nat. Photonics **15**, 530 (2021).
- [30] J.-P. Chen, C. Zhang, Y. Liu, C. Jiang, W.-J. Zhang, Z.-Y. Han, S.-Z. Ma, X.-L. Hu, Y.-H. Li, H. Liu, F. Zhou, H.-F. Jiang, T.-Y. Chen, H. Li, L.-X. You, Z. Wang, X.-B. Wang, Q. Zhang, and J.-W. Pan, Twin-field quantum key distribution over a 511 km optical fibre linking two distant metropolitan areas, Nat. Photonics **15**, 570 (2021).
- [31] S. Wang, Z.-Q. Yin, D.-Y. He, W. Chen, R.-Q. Wang, P. Ye, Y. Zhou, G.-J. Fan-Yuan, F.-X. Wang, Y.-G. Zhu, P. V. Morozov, A. V. Divochiy, Z. Zhou, G.-C. Guo, and Z.-F. Han, Twin-field quantum key distribution over 830-km fibre, Nat. Photonics **16**, 154 (2022).
- [32] K. Tamaki, M. Curty, G. Kato, H.-K. Lo, and K. Azuma, Loss-tolerant quantum cryptography with imperfect sources, Phys. Rev. A **90**, 052314 (2014).
- [33] F. Xu, K. Wei, S. Sajeed, S. Kaiser, S. Sun, Z. Tang, L. Qian, V. Makarov, and H.-K. Lo, Experimental quantum key distribution with source flaws, Phys. Rev. A **92**, 032305 (2015).
- [34] Z. Tang, K. Wei, O. Bedroia, L. Qian, and H.-K. Lo, Experimental measurement-device-independent quantum key distribution with imperfect sources, Phys. Rev. A **93**, 042308 (2016).
- [35] M. Pereira, M. Curty, and K. Tamaki, Quantum key distribution with flawed and leaky sources, npj Quantum Inf. **5**, 62 (2019).
- [36] S. L. Braunstein and S. Pirandola, Side-channel-free quantum key distribution, Phys. Rev. Lett. **108**, 130502 (2012).
- [37] Z.-Q. Yin, C.-H. F. Fung, X. Ma, C.-M. Zhang, H.-W. Li, W. Chen, S. Wang, G.-C. Guo, and Z.-F. Han, Measurement-device-independent quantum key distribution with uncharacterized qubit sources, Phys. Rev. A **88**, 062322 (2013).
- [38] S. Sun, Security of reference-frame-independent quantum key distribution with source flaws, Phys. Rev. A **104**, 022423 (2021).
- [39] X.-B. Wang, X.-L. Hu, and Z.-W. Yu, Practical long-distance side-channel-free quantum key distribution, Phys. Rev. Applied **12**, 054034 (2019).
- [40] H.-W. Li, Z.-Q. Yin, W. Chen, S. Wang, G.-C. Guo, and Z.-F. Han, Quantum key distribution based on quantum dimension and independent devices, Phys. Rev. A **89**, 032302 (2014).
- [41] H.-J. Ding, X.-Y. Zhou, C.-H. Zhang, J. Li, and Q. Wang, Measurement-device-independent quantum key distribution with insecure sources, Opt. Lett. **47**, 665 (2022).
- [42] M. Pereira, G. Kato, A. Mizutani, M. Curty, and K. Tamaki, Quantum key distribution with correlated sources, Sci. Adv. **6**, eaaz4487 (2020).
- [43] A. Navarrete, M. Pereira, M. Curty, and K. Tamaki, Practical quantum key distribution that is secure against side channels, Phys. Rev. Applied **15**, 034072 (2021).
- [44] C. Zhang, X.-L. Hu, J.-P. Chen, Y. Liu, W. Zhang, Z.-W. Yu, H. Li, L. You, Z. Wang, X.-B. Wang, *et al.*, Experimental side-channel-free quantum key distribution, arXiv preprint [arXiv:2103.06058](https://arxiv.org/abs/2103.06058) (2021).
- [45] H.-K. Lo and J. Preskill, Security of quantum key distribution using weak coherent states with nonrandom phases, Quantum Inf. Comput. **7**, 431 (2007).
- [46] M. Koashi, Simple security proof of quantum key distribution based on complementarity, New J. Phys. **11**, 045018 (2009).
- [47] W.-B. Liu, C.-L. Li, Y.-M. Xie, C.-X. Weng, J. Gu, X.-Y. Cao, Y.-S. Lu, B.-H. Li, H.-L. Yin, and Z.-B. Chen, Homodyne detection quadrature phase shift keying continuous-variable quantum key distribution with high excess noise tolerance, PRX Quantum **2**, 040334 (2021).
- [48] V. Zapatero, Á. Navarrete, K. Tamaki, and M. Curty, Security of quantum key distribution with intensity correlations, Quantum **5**, 602 (2021).
- [49] K.-i. Yoshino, M. Fujiwara, K. Nakata, T. Sumiya, T. Sasaki, M. Takeoka, M. Sasaki, A. Tajima, M. Koashi, and A. Tomita, Quantum key distribution with an efficient countermeasure against correlated intensity fluctuations in optical pulses, npj Quantum Inf. **4**, 8 (2018).
- [50] V. Scarani and R. Renner, Quantum cryptography with finite resources: Unconditional security bound for discrete-variable protocols with one-way postprocessing,

- Phys. Rev. Lett. **100**, 200501 (2008).
- [51] W. Hoeffding, Probability inequalities for sums of bounded random variables, J. Am. Stat. Assoc. **58**, 13 (1963).
  - [52] H.-L. Yin, M.-G. Zhou, J. Gu, Y.-M. Xie, Y.-S. Lu, and Z.-B. Chen, Tight security bounds for decoy-state quantum key distribution, Sci. Rep. **10**, 14312 (2020).
  - [53] K. Maeda, T. Sasaki, and M. Koashi, Repeaterless quantum key distribution with efficient finite-key analysis overcoming the rate-distance limit, Nat. Commun. **10**, 3140 (2019).
  - [54] G. Currás-Lorenzo, Á. Navarrete, K. Azuma, G. Kato, M. Curty, and M. Razavi, Tight finite-key security for twin-field quantum key distribution, npj Quantum Inf. **7**, 22 (2021).
  - [55] X. Zhong, J. Hu, M. Curty, L. Qian, and H.-K. Lo, Proof-of-principle experimental demonstration of twin-field type quantum key distribution, Phys. Rev. Lett. **123**, 100506 (2019).
  - [56] H.-L. Yin and Y. Fu, Measurement-device-independent twin-field quantum key distribution, Sci. Rep. **9**, 3045 (2019).
  - [57] M. Lucamarini, I. Choi, M. B. Ward, J. F. Dynes, Z. L. Yuan, and A. J. Shields, Practical security bounds against the trojan-horse attack in quantum key distribution, Phys. Rev. X **5**, 031030 (2015).
  - [58] G. Zhang, I. W. Primaatmaja, J. Y. Haw, X. Gong, C. Wang, and C. C. W. Lim, Securing practical quantum communication systems with optical power limiters, PRX Quantum **2**, 030304 (2021).
  - [59] A. Mizutani, G. Kato, K. Azuma, M. Curty, R. Ikuta, T. Yamamoto, N. Imoto, H.-K. Lo, and K. Tamaki, Quantum key distribution with setting-choice-independently correlated light sources, npj Quantum Inf. **5**, 8 (2019).
  - [60] F. Xu, K. Wei, S. Sajeed, S. Kaiser, S. Sun, Z. Tang, L. Qian, V. Makarov, and H.-K. Lo, Experimental quantum key distribution with source flaws, Phys. Rev. A **92**, 032305 (2015).
  - [61] Z. Yuan, B. Fröhlich, M. Lucamarini, G. Roberts, J. Dynes, and A. Shields, Directly phase-modulated light source, Phys. Rev. X **6**, 031044 (2016).
  - [62] I. De Marco, R. I. Woodward, G. L. Roberts, T. K. Paraíso, T. Roger, M. Sanzaro, M. Lucamarini, Z. Yuan, and A. J. Shields, Real-time operation of a multi-rate, multi-protocol quantum key distribution transmitter, Optica **8**, 911 (2021).

## Supplementary Materials for Experimental twin-field quantum key distribution with flawed and correlated sources

### section S1. Formula of the final key rate

In our four-phase twin-field QKD protocol, the classical bits can be encoded through phase differences of coherent pulses from Alice and Bob and the setting of the X and Y bases introduces the idea of "quantum coin" where we can introduce  $\Delta$  as the imbalance of a quantum coin to bound the information leakage. The imbalance  $\Delta$  can be calculated through the bounded fidelity discussed in the GLLP security proof [45, 46], which can be naturally extended to the security analysis of the RT [42]. In the ideal scenario with no source flaws, Alice's entangled basis-dependent states are expressed as

$$\begin{aligned} |\Psi_X\rangle_{Aa} &= \frac{1}{\sqrt{2}}(|0_X\rangle_A |\alpha\rangle_a + |1_X\rangle_A |-\alpha\rangle_a), \\ |\Psi_Y\rangle_{Aa} &= \frac{1}{\sqrt{2}}(|1_Y\rangle_A |i\alpha\rangle_a + |0_Y\rangle_A |-i\alpha\rangle_a), \end{aligned} \quad (S1)$$

where  $\{|0_X\rangle, |1_X\rangle\}$  are eigenstates of the Pauli operator  $\sigma_x$  and  $\{|0_Y\rangle, |1_Y\rangle\}$  are eigenstates of the Pauli operator  $\sigma_y$ . The same equations of Bob's entangled basis-dependent states can be obtained in the similar expressions with the system B denoting the virtual qubit space and the system b representing the actual space of coherent pulses. Here, the basis-dependence of Alice's (Bob's) entangled states can be related to an equivalent virtual protocol considering the balance of a quantum coin [45], where Alice (Bob) measures the coin in the Z basis to determine the basis choice. Here the basis-dependent states can be expressed as  $|\Psi_X\rangle$  and  $|\Psi_Y\rangle$  without distinguishing the sender. The joint state can be taken to be

$$|\Phi\rangle = \sqrt{p_x}|0_Z\rangle|\Psi_X\rangle + \sqrt{p_y}|1_Z\rangle|\Psi_Y\rangle, \quad (S2)$$

where  $p_x$  and  $p_y$  separately represent the probabilities of sending states in the X basis and the Y basis. Note that we assume the measurement of the quantum coin will be delayed after Charlie has finished her measurement and eavesdropping. The final key rate of this protocol is

$$R = Q^x[1 - fH(E_b^x) - H(E_p)], \quad (S3)$$

where  $Q^x = (1 - p_d)[1 - (1 - 2p_d)e^{-2\eta|\alpha|^2}]$  and  $E_b^x Q^x = e_{d_x}(1 - p_d)[1 - (1 - p_d)e^{-2\eta|\alpha|^2}] + (1 - e_{d_x})p_d(1 - p_d)e^{-2\eta|\alpha|^2}$ .  $Q^x$  is the gain in the X basis and  $E_b^x$  means the bit error rate under the X basis.  $e_{d_x}$  means the misalignment error rate in the X basis of the four-phase twin-field QKD system. The total efficiency is  $\eta$  and we use  $|\alpha|^2$  to express the intensity of weak coherent states.  $E_p$  represents the phase error rate under the X basis, which is bounded by  $\Delta$  and the bit error rate in the Y basis  $E_b^y$ . The equation of  $E_b^y$  is similar to that of  $E_b^x$  with its separate misalignment error rate  $e_{d_y}$  that  $E_b^y Q = e_{d_y}(1 - p_d)[1 - (1 - p_d)e^{-2\eta|\alpha|^2}] + (1 - e_{d_y})p_d(1 - p_d)e^{-2\eta|\alpha|^2}$ .

Here for simulation, we just consider the situation that  $E_b^y$  is equal to  $E_b^x$  since we set the misalignment error rates to be 0 without the finite-key analysis. Note that  $E_b^y$  is not rigorously equal to  $E_b^x$  in the practical scenario since  $e_{d_y}$  evidently differs from  $e_{d_x}$  in experiment.  $\eta = \eta_d \times 10^{-L/20}$ , where  $L$  (dB) is the total attenuation of the channel.

Based on the fact that our protocol considers an biased basis choice, we provide the relation between the phase error rate in the X basis  $E_p$  and the bit error rate in the Y basis  $E_b^y$ . According to the procedure of our protocol, the simplified entangled state shared by Alice and Bob in two bases can be expressed as

$$\begin{aligned} |X\rangle &= |\Psi_X\rangle_{Aa} |\Psi_X\rangle_{Bb}, \\ |Y\rangle &= |\Psi_Y\rangle_{Aa} |\Psi_Y\rangle_{Bb}, \end{aligned} \quad (S4)$$

where we denote regardless of the measurement result of Charlie. We introduce the error operator by Alice and Bob,  $E_{AB}^y = |0_Y 1_Y\rangle_{AB} \langle 0_Y 1_Y| + |1_Y 0_Y\rangle_{AB} \langle 1_Y 0_Y|$ . The phase error rate of the X basis and the bit error rate of the Y basis are defined as

$$\begin{aligned} E_p &= \langle X| M_{ab}^\dagger E_{AB}^y M_{ab} |X\rangle, \\ E_b^y &= \langle Y| M_{ab}^\dagger E_{AB}^y M_{ab} |Y\rangle, \end{aligned} \quad (S5)$$

where  $M_{ab}$  is the Kraus operator corresponding to the announcement of Charlie. Note that the normalization has been assumed. Similar with the method in Ref. [38], we have

$$\begin{aligned} E_p &= |\langle X|Y\rangle|^2 \langle Y| \mathbf{E} |Y\rangle + |\langle X|Y^\perp\rangle|^2 \langle Y^\perp| \mathbf{E} |Y^\perp\rangle \\ &\quad + \langle X|Y\rangle \langle X|Y^\perp\rangle (\langle Y| \mathbf{E} |Y^\perp\rangle + \langle Y^\perp| \mathbf{E} |Y\rangle), \end{aligned} \quad (S6)$$

where we let  $\mathbf{E} = M_{ab}^\dagger E_{AB}^y M_{ab}$  and use the fact that  $I = |Y\rangle \langle Y| + |Y^\perp\rangle \langle Y^\perp|$ . The fidelity of quantum states can be expressed as  $1 - 2\Delta' = \langle X|Y\rangle = |\langle \Psi_X | \Psi_Y \rangle|^2$ . Eve can enhance the source flaws by exploiting the loss of channel, which means that we should have the the worst situation  $\Delta = \Delta'/Q$  [45]. Therefore, we can obtain the relation between  $E_b^y$  and  $\Delta$ ,

$$1 - 2\Delta \leq \sqrt{E_b^y E_p} + \sqrt{(1 - E_b^y)(1 - E_p)}. \quad (S7)$$

### section S2. Finite-key analysis for the experimental implementation

Here we provide the specific expression of the finite-key analysis for the experiment of our protocol. The security of the final key rate is against collective attacks, based on the method in Ref. [50]. Note that the security against coherent attacks has already been proposed and accommodates the same method here [53, 54]. We here just consider collective attacks for simplicity. The number of



final key bits  $l$  has been expressed as

$$l = n_x \left[ 1 - H(\bar{E}_p) - \text{leak}_{\text{EC}} - 7 \sqrt{\frac{\log_2(2/\bar{\epsilon})}{n_x}} - \frac{1}{n_x} \log_2 \frac{2}{\epsilon_{\text{EC}}} - \frac{2}{n_x} \log_2 \frac{1}{\epsilon_{\text{PA}}} \right]. \quad (\text{S8})$$

We directly offer  $n_x$  through the experiment, together with  $E_b^X$  in the formula of  $\text{leak}_{\text{EC}}$ . The statistical fluctuation applied to calculate  $\bar{E}_p$  will be presented to finish our finite-key analysis. First, we set  $n_y$  and  $m_y$  to be the number of efficient outcomes and the number of bit errors in the Y basis, which is obtained through the experiment. Using the Hoeffding inequality [51], we derive an upper bound of the expectation value of the number of bit errors in the Y basis  $m_y^*$ . The upper bound of the expected bit error rate in the Y basis is  $E_b^{y*} = m_y^*/n_y$ , which can be used to calculate the upper bound of the expected value of the phase error rate in the X basis  $E_p^*$ . Then the number of phase errors is obtained in the form of  $m_p^* = n_x E_p^*$ . We then estimate the upper bound of the observed number of phase errors in the X basis  $\bar{m}_p$  through Chernoff bound [52]. Then  $\bar{E}_p$  can be naturally calculated with  $\bar{E}_p = \bar{m}_p/n_x$ . Formulas of Hoeffding inequality and Chernoff bound are listed as follows,

$$m_y^* = m_y + \sqrt{\frac{m_y \beta}{2}}, \quad (\text{S9})$$

$$\bar{m}_p = \left( 1 + \frac{\beta + \sqrt{8m_p^* \beta + \beta^2}}{2m_p^*} \right) m_p^*,$$

where  $\beta = -\ln(\epsilon_F)$  and  $\epsilon_F$  represents the failure probability introduced in the Chernoff bound. Without loss of generality, we set all failure probabilities  $\epsilon_{\text{EC}} = \epsilon_{\text{PA}} = \bar{\epsilon} = \epsilon_F = 10^{-10}$ .

### section S3. Intensity fluctuation

Imperfect intensity modulation can be quantitatively characterized by the value of intensity fluctuation over a period of time. We divide the fluctuation into two parts, the source fluctuation and the path fluctuation. For the source part, we directly measured the intensity of the laser source with a 40 dB attenuation. Since the circulator and beam splitters used in the system are igfast-axis blocked, changes in polarization bring about fluctuations in intensity. Consequently, we measured the intensity of pulses sent by Alice with an appropriate attenuation to make the intensity around -70 dBm while the phase modulations are carried on. Besides, VOA also causes intensity fluctuation, so we add an additional attenuation each to the measurement of the fluctuation of path and source, which means the intensity of these pulses is lower than the minimum intensity we sent when considering source flaws. As shown in fig. S1, the upper bound of intensity fluctuation is 1.17% (0.048 dB).

### section S4. Phase shift

We quantify the modulation error  $\delta$  in the source through calibrating Alice's PM, in the plug-and-play QKD system.  $\delta_\phi$  is defined as the difference between the actual phase and the expected phase  $\phi$ . In our protocol, we need to modulate 4 phases  $\phi \in \{0, \pi/2, \pi, 3\pi/2\}$ . Similar to Ref. [60], only Alice performs phase modulation and Bob sets his own PM at a fixed unmodulated phase 0. Alice scans the voltages applied to her PM according to the random phase selection in the experiment and the intensity of these pulses is 0.001. Charlie records the clicks for 100 seconds. Based on the phase selection, we can obtain the number of clicks for different phases and these counts are denoted by  $D_1^\phi$  and  $D_2^\phi$ . For  $D_1$ , the total detection efficiency  $\eta_1$  (considering the loss in Charlie) is 66.3% and the dark count rate  $p_{d,1}$  is  $1.6 \times 10^{-8}$ . For  $D_2$ , the detection efficiency  $\eta_2$  is 73.6% and the dark count rate  $p_{d,2}$  is  $2.5 \times 10^{-8}$ . Since the dark count rates of two detectors are at the level of  $10^{-8}$ , dark counts have little influence on the computation and are ignored in the computation. The electrical driver used is DR-VE-10-MO (iXblue). In our data analysis, we use Hoeffding's inequality [51]. The upper bound of  $\delta_\phi$  is given by Eq. (S10). For  $\phi \in \{\pi/2, \pi\}$ ,  $\phi_0 = \phi$  and for  $\phi = 3\pi/2$ ,  $\phi_0 = \phi - \pi$ .

The upper bounds of different phases are shown in table S1. From this table, the error  $\delta$  is upper bounded by the case of  $\bar{\delta}_\pi = 0.062$ .

### section S5. Polarization contrast

Since Eve could distinguish signals from the polarization information of each state, we quantify this situation by measuring the polarization contrast in the plug-and-play system. We put a polarization beam splitter (PBS) at Alice's site to obtain the polarization contrast of the pulses Alice sent. As shown in fig. S2, we measured the contrast for 1000 seconds and the minimum value is still over 26.5 dB. As we only need 100 seconds to perform a round of measurement, the polarization contrast can be easily maintained above 26.5 dB.

### section S6. Pattern effect

Practical electro-optic modulators and electrical drivers are band limited, which results in state correlation between the optical pulses as well as intensity fluctuation of individual pulses. State correlation is particularly critical for the security since current security analysis usually assumes independent and identically distributed pulses. In this experiment, we do not need to modulate different intensities and we only need to quantify the phase correlation. Almost all the influences of pattern effects are limited to the adjacent pulses [49]. Consequently, for four phases, sixteen patterns exist. We quantified the phase correlation by measuring the intensities under different patterns. Bob's PM is set at an unmodulated phase 0 and Alice modulates each pattern with equal probability. The modulated pulses and unmodulated pulses interfere

$$\bar{\delta}_\phi = \max \left\{ \left| \phi_0 - 2\arctan \sqrt{\frac{(\bar{D}_{2,\phi}^* - \underline{D}_{2,0}^*)/\eta_2}{(\bar{D}_{1,\phi}^* - \bar{D}_{2,0}^*)/\eta_1}} \right|, \left| \phi_0 - 2\arctan \sqrt{\frac{(\underline{D}_{2,\phi}^* - \bar{D}_{2,0}^*)/\eta_2}{(\bar{D}_{1,\phi}^* - \underline{D}_{2,0}^*)/\eta_1}} \right| \right\}, \quad (\text{S10})$$

at BS and the results are measured by D1 and D2 with detection efficiencies of 66.3% and 73.6%. Denote phase 0 as  $S_1$ , phase  $\pi/2$  as  $S_2$ , phase  $\pi$  as  $S_3$  and phase  $3\pi/2$  as  $S_4$ . The pattern effects of phase 0 and  $\pi/2$  are given by D1's detection results while the pattern effects of phase  $\pi$  and  $3\pi/2$  are given by D2's detection results. As shown in table S2, the maximum value is  $8.54 \times 10^{-3}$ .

### section S7. Scheme with independent lasers

We extend the plug-and-play system to a scheme with independent lasers in this part. As shown in fig. S3, this system includes two independent users and an untrusted intermediate node.

The phase-modulated pulses are directly generated employing the idea of optical injection [61, 62]. Alice's (Bob) laser source is made up with a phase-preparation laser (PP-Laser) and a pulse-generation laser (PG-Laser). Two laser diodes are connected with an optical circulator. PP-Laser acts as a master laser and PG-Laser acts as a slave laser. The phase encoding laser is always biased over its threshold to produce continuous-wave (CW) emission and a small current modulation, synchronized to the interval of two injection locked pulses, is applied when a phase modulation is required. The relative phase between the secondary pulses depends on the phase evolution of the primary pulses and can be set to an arbitrary value by directly modulating the driving current applied to PP-Laser. Bob locks his PP-Laser to Alice's PP-Laser by utilizing an optical phase-locked loop (OPLL). The modulated optical pulses are then attenuated to the single-photon level by a variable optical attenuator and their intensities are monitored by detectors. A polarizer is used to improve the polarization contrast of pulses sent.

After traveling through optical fibers, Alice's and Bob's pulses interfere with each other on Charlie's BS. Two polarization controllers (PCs) are used to modify the polarization of the incident pulses to achieve the maximum detection efficiencies. One feedback phase modulator (PM) is added in the path from Alice to Charlie's BS to compensate for the relative phase drift introduced by fiber channels. The interference results are finally detected by two superconducting single-photon detectors, D1 and D2.

Since our protocol does not need intensity modulation, this scheme removes the need for electro-optic modulators and electrical drivers, simplifying the experiment. Moreover, our protocol can resist Trojan horse attacks in this system. Here, we propose a scheme that two in-

dependent parties share secure keys considering source flaws with developed technology, which can be widely implemented in the approaching quantum networks.

### section S8. Experimental results

We summarized the optical element transmittance in table S3. The optical elements include the polarization controllers (PCs), circulator (CIR), and the beam splitter (BS). The results are given for each output (D1/D2) as appropriate.

The experimental results are summarized in table S4, the total pulses sent in the experiment N, the phase error rate regardless the source flaws  $E_P^*$ , the phase error rate considering the source flaws  $E_P$ , the number of detected pulses is labeled as "Detected-AB (Di)", where "A" ("B") means an A (B) phase was added on the pulses by Alice (Bob) and detected by Di,  $i \in \{1, 2\}$ . For 30 dB and 35 dB, the key rates are 0 and  $E_P = 50\%$ .

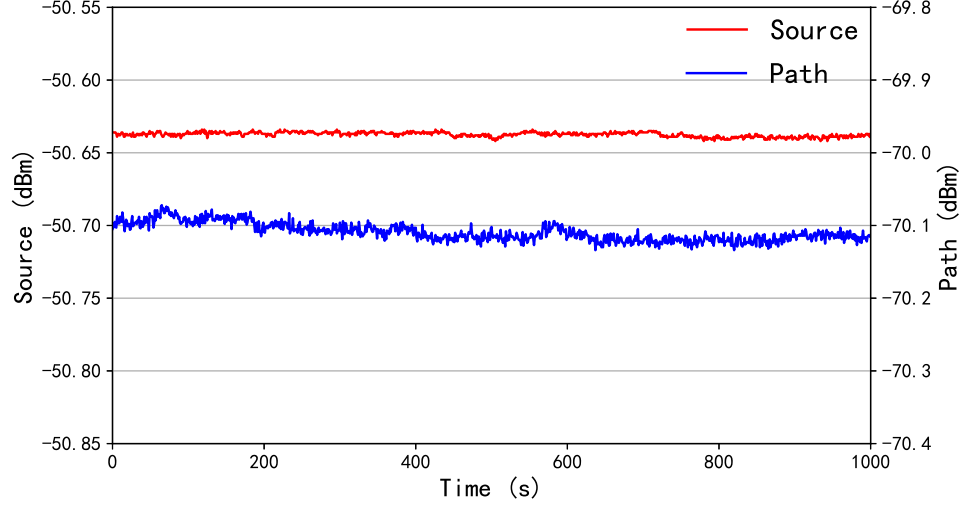


**fig . S1. Intensity fluctuation.** We divide the intensity fluctuation into two parts, the source fluctuation and the path fluctuation. We measure the fluctuation for 1000 seconds. Red line reflects the fluctuation of the source and the maximum difference within 100 s is 0.008 dB. While the blue line reflects the fluctuation of the path and the maximum value is 0.04 dB.

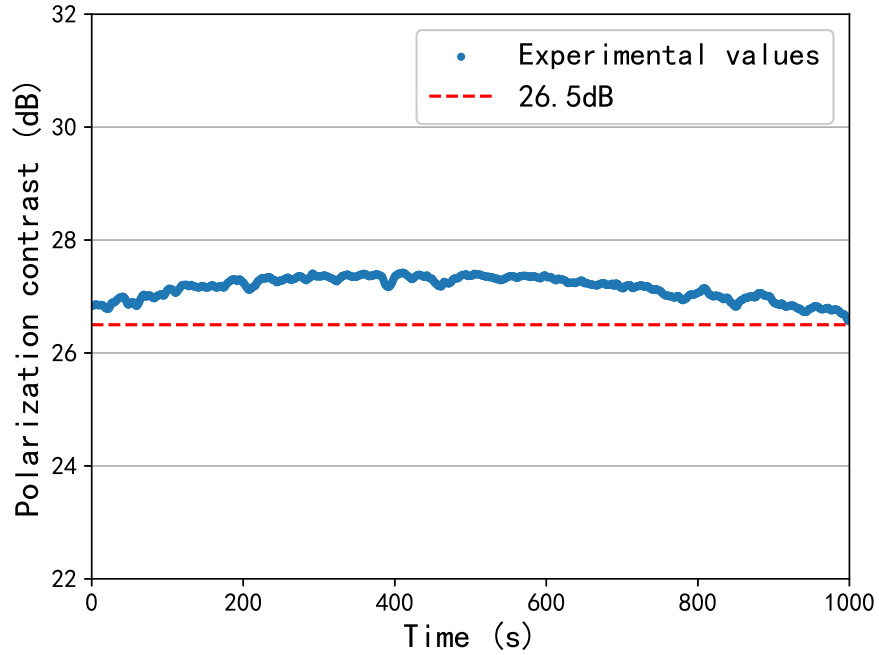


**fig . S2. Polarization contrast versus time.** We measured the polarization contrast of Alice's and Bob's pulses by a polarization beam splitter (PBS) for 1000 seconds while our system considering realistic sources, only runs for 100 seconds. Its value is always above 26.5 dB.

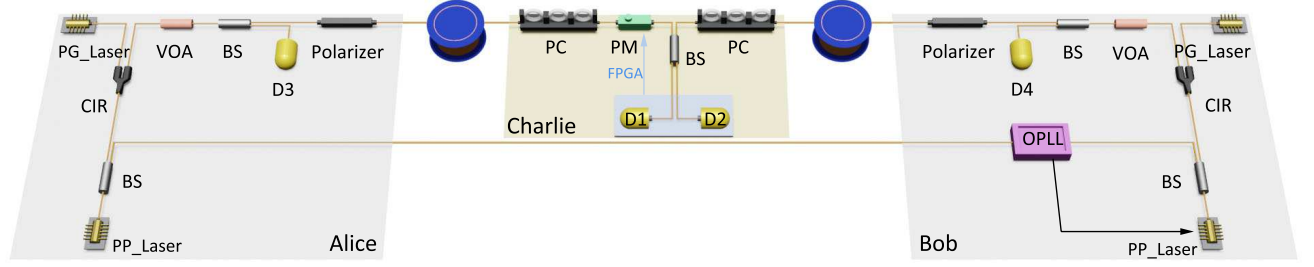


**fig . S3. Experimental setup of two independent users.** The phase-modulated pulses are generated by light sources without phase modulators. The light source consists of a phase-preparation laser (PP-Laser) and a pulse-generation laser (PG-Laser). PG-Laser is connected to PP-Laser via an optical circulator (CIR). Bob owns an optical phase-locked loop (OPLL) to lock his PP-Laser to Alice's PP-Laser. After traveling through quantum channels, Alice's and Bob's encoded pulses interfere with each other on Charlie's beam splitters (BS), and are finally detected by two superconducting nanowire single-photon detectors, D1 and D2. EPC, electrical polarization controller; VOA, variable optical attenuator; PC, polarization controller; PM, phase modulator.

**table . S1. Upper bounds of different phases.** The number of clicks detected by  $D_1$  and  $D_2$  under different phases and their upper bound  $\bar{\delta}_\phi$ .

$\phi$	$D_{1,\phi}$	$D_{2,\phi}$	$\bar{\delta}_\phi$
0	5956406	1269	-
$\pi/2$	343663	376778	0.012
$\pi$	6627	6597672	0.062
$3\pi/2$	333491	367139	0.010

**table . S2. Detection clicks of pulses with different phases for sixteen types of predecessors.**

Pattern	Counts of second pulse	deviation from the average value
$S_1 \rightarrow S_1$	411665	$1.54 \times 10^{-3}$
$S_2 \rightarrow S_1$	412610	$7.52 \times 10^{-4}$
$S_3 \rightarrow S_1$	411939	$8.76 \times 10^{-4}$
$S_4 \rightarrow S_1$	412986	$1.66 \times 10^{-3}$
$S_1 \rightarrow S_2$	206867	$5.61 \times 10^{-4}$
$S_2 \rightarrow S_2$	208191	$6.96 \times 10^{-3}$
$S_3 \rightarrow S_2$	206554	$8.08 \times 10^{-4}$
$S_4 \rightarrow S_2$	205362	$6.72 \times 10^{-3}$
$S_1 \rightarrow S_3$	455404	$2.93 \times 10^{-3}$
$S_2 \rightarrow S_3$	454520	$9.83 \times 10^{-4}$
$S_3 \rightarrow S_3$	452736	$2.95 \times 10^{-3}$
$S_4 \rightarrow S_3$	453635	$9.66 \times 10^{-4}$
$S_1 \rightarrow S_4$	227822	$6.37 \times 10^{-3}$
$S_2 \rightarrow S_4$	227191	$3.58 \times 10^{-3}$
$S_3 \rightarrow S_4$	226059	$1.42 \times 10^{-3}$
$S_4 \rightarrow S_4$	224446	$8.54 \times 10^{-3}$

**table . S3. Efficiencies of measurement station.**

Optical devices	Attenuation
CIR 2→3	0.62 dB
BS-1	0.47 dB
BS-2	0.45 dB
PC-1	0.18 dB
PC-2	0.16 dB



**table . S4. Experimental results obtained under different losses**

Channel loss	10 dB	16 dB	20 dB	30 dB	35 dB
N	$10^{10}$	$10^{10}$	$10^{10}$	$10^{10}$	$10^{10}$
$E_p^*$	16.4%	15.8%	13.6%	17.8%	18.3%
$E_p$	21.4%	26.5%	32.4%	50.0%	50.0%
Detected 00 (D1)	11697938	2700313	882175	108166	29340
Detected 0 $\pi$ (D1)	36848	9031	2703	261	113
Detected $\pi$ 0 (D1)	23186	6897	1994	319	73
Detected $\pi\pi$ (D1)	11633036	2699790	882851	108459	29303
Detected $\frac{\pi}{2}\frac{\pi}{2}$ (D1)	143957	33188	10872	1773	472
Detected $\frac{\pi}{2}\frac{3\pi}{2}$ (D1)	491	108	35	5	3
Detected $\frac{3\pi}{2}\frac{\pi}{2}$ (D1)	603	162	45	8	3
Detected $\frac{3\pi}{2}\frac{3\pi}{2}$ (D1)	143048	33308	10766	1284	331
Detected 00 (D2)	7516	1693	570	106	65
Detected 0 $\pi$ (D2)	12982085	2998179	973757	121242	31961
Detected $\pi$ 0 (D2)	12973080	2996549	971129	125848	33099
Detected $\pi\pi$ (D2)	45002	8655	2994	590	163
Detected $\frac{\pi}{2}\frac{\pi}{2}$ (D2)	347	60	20	4	1
Detected $\frac{\pi}{2}\frac{3\pi}{2}$ (D2)	167242	38832	12464	1543	408
Detected $\frac{3\pi}{2}\frac{\pi}{2}$ (D2)	167263	38658	12650	1348	346
Detected $\frac{3\pi}{2}\frac{3\pi}{2}$ (D2)	823	216	71	8	2